

Time- and space-resolved dynamic studies on ceramic and cementitious materials

Paul Barnes,^{a*} Sally Colston,^a Bernadette Craster,^b Chris Hall,^{b†} Andrew Jupe,^a Simon Jacques,^a Jeremy Cockcroft,^a Shane Morgan,^a M. Johnson,^a D. O'Connor^a and M. Bellotto^c

^aIndustrial Materials Group, Department of Crystallography, Birkbeck College, Malet Street, London WC1E 7HX, UK, ^bSchlumberger Cambridge Research Ltd, High Cross, Madingley Road, Cambridge CB3 0EL, UK, and ^cCTG Italcementi Group, Rue des Technodes, 78931 Guerville, France. E-mail: barnes@img.cryst.bbk.ac.uk

(Received 20 January 2000; accepted 28 February 2000)

A review is given of the results and lessons arising from a sustained *in situ* diffraction study of the structure and performance of functional ceramic/cementitious materials in which synchrotron-based energy-dispersive diffraction has been the central under-pinning technique. Five particular points of discussion emerge: the demands on time resolution; the use of penetrating radiation for the *in situ* mode; the need for complementary techniques; re-analysing of data; spatially resolved diffraction: a new tomography. These aspects are discussed in turn using illustrative examples taken from the fields of cement hydration, clay intercalation, cation-exchanged zeolites, and particulate/fluid invasion into building and archaeological objects.

Keywords: diffraction; tomography; cements; ceramics.

1. Time resolution

Rapid data collection has been a long-standing pursuit of the synchrotron and neutron radiation communities; spectacular time resolutions, approaching hundreds of femtoseconds, have been obtained in highly specialized situations (e.g. Wark, 1999). The experience gained within these studies on bulk solid-state chemistry systems is that the most frequently needed time resolutions lie in the 1 s to 5 min timescale, which is conveniently well matched to the performance of current conventional energy-dispersive detector systems (useful count rates in the 10^4 – 10^5 counts s^{-1} range). Synchrotron-based angle-scanning (monochromatic) diffraction is now also capable of delivering sub-minute powder patterns of sufficient quality sometimes for Rietveld structure refinement (e.g. Svensson *et al.*, 1997; Norby *et al.*, 1999). Thus the distinguishing advantages of the energy-dispersive diffraction (EDD) method lie mainly in flexibility with respect to complex specimen environments and very short timescales (1 s or less). In the following we present two illustrative examples where these two attributes were essential.

1.1. Intercalation of clays

Research into the fundamentals of hydration and intercalation in swelling clays is an important topic for the oil industry. It has led to significant advances in the technology

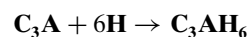
of shale stabilization during drilling (Boek *et al.*, 1998) and gives new insight into the diagenesis of clays and their behaviour under reservoir conditions (De Siqueira *et al.*, 1999). Molecular modelling of the interlayer space in the presence of water, ions (Boek *et al.*, 1995) and intercalation species such as polyglycols (Boek *et al.*, 1998) has been used successfully in interpreting high-quality neutron diffraction data (Skipper *et al.*, 1995). *In situ* EDD has also become accepted as a valuable adjunct (Redfern, 1987; Bray & Redfern, 1999; Fogg & O'Hare, 1999) to more traditional methods (e.g. neutron and conventional diffraction, thermo-gravimetric techniques) for studying intercalation within layered minerals (e.g. kaolinite, montmorillonite, gibbsite) providing data for kinetic analysis (use of rate equations and Arrhenius plots) and elucidating the reaction pathways (presence of intermediates *etc.*). In the case presented here it turns out that the ability with EDD to be able to spatially resolve the intercalation has been a key additional feature. For example, very rapid changes in interlayer spacing have been observed when an 8 wt% KCl solution is injected (*via* a remotely controlled solenoid valve) into a stirred suspension of Na-montmorillonite pretreated with polyglycol. The reduction of basal spacing from 1.8 to 1.5 nm corresponds to the removal of one layer of water molecules. In this experiment, EDD patterns were collected in 1 s at intervals of 7 s (Fig. 1a). Such ion-exchange experiments can be carried out on dilute suspensions, typical of processes occurring in colloidal clay aggregates in dilute suspension, as well as in dense clay

† Now at Centre for Materials Science and Engineering, University of Edinburgh, Edinburgh EH9 3JL, UK.

pastes. Furthermore, the idea has been explored of time-resolving such rapid sequences by using a spatially dispersed continuous system, following an approach used previously to follow continuous polymer processing (Ryan, 1999). This exploits the fine spatial resolution of the EDD method (with a collimated beam of width $\sim 50\mu\text{m}$) to track the penetration of species into a montmorillonite clay film in a purpose-built osmotic cell (Craster, 1999). The osmotic cell consists of two compartments each containing 20 ml solutions of different composition (e.g. sodium and potassium chloride) connected by a thin ($150\mu\text{m}$ -thick) clay film held between two circular sintered glass plates of diameter 25 mm. The EDD-tomographic technique is used to observe the variation of d -spacing across the connecting length of the film in steps of $10\mu\text{m}$, thus separating the original and reduced basal spacings (Fig. 1b). These methods, in which the kinetic and spatial capabilities of EDD are combined, appear to hold great promise for direct observation of phenomena in reactors and continuous processing equipment.

1.2. Hydration of tricalcium aluminate

The need for time resolution in the study of the hydration of tricalcium aluminate has already been identified (Jupe *et al.*, 1996) though this example is worthy of reconsideration. In the absence of sulfate compounds, tricalcium aluminate will rapidly hydrate to a stable hydrate known as C_3AH_6 (Roberts, 1957; Buttler *et al.*, 1959) at ambient or higher temperatures. This simple viewpoint can be represented by the following reaction equation,



where $\text{C} = \text{CaO}$, $\text{A} = \text{Al}_2\text{O}_3$, $\text{H} = \text{H}_2\text{O}$.

The reaction has been well studied using conventional X-ray diffraction (Roberts, 1957; Buttler *et al.*, 1959), transmission electron microscopy (e.g. Kolbasov *et al.*, 1980) and wet chemical analysis of the liquid phase (e.g. Glasser & Marinho, 1985). The accepted view is that the dissolution of C_3A is rapid and incongruent and that the closely related unstable hydrates, C_2AH_8 and C_4AH_{19} , are also involved in the process either as competing hydrate products, through topotactic transformations on the outer layers or 'skin' of C_3A grains, or as intermediate phases prior to crystallization of C_3AH_6 from solution; the latter view has been proposed by Stein (1980). It was against this background that the previously reported results (Jupe *et al.*, 1996), using remote-controlled feed/mixing hydration experiments on beamline ID9 of the ESRF in EDD-mode, unambiguously showed that the C_3A hydration sequence, regardless of temperature and rapidity, always involves a short-lived intermediate phase believed to be the unstable hydrate C_2AH_8 (or the closely related C_4AH_{19}). This intermediate was interpreted as a necessary nucleating phase for the subsequent C_3AH_6 growth and the capture of its fleeting presence was correctly attributed to the time resolutions (0.35 and 6 s, respectively) used in the experiment; the sequence is illustrated here by the normalized phase plot of Fig. 2(a). The additional importance of the spatial resolution used (effective diffraction cross section of $40 \times 40\mu\text{m}$) has now become more apparent. Since the hydration proceeds during normal measurement with a continuous range of reaction rates, corresponding to unavoidable variations in temperature and water ingress throughout the bulk specimen, conventional *in situ* diffraction will obtain a view of the sequence smeared by the combined effects of inferior time resolution and specimen broadening; this situation is analogous to the well known instrumental and specimen contributions to peak broadening in powder diffraction. The effect can be simulated by integrating a continuous range of plots over varied time windows (Fig. 2). Even after just 50 s of time-smearing the $\text{C}_3\text{A} \rightarrow$ intermediate $\rightarrow \text{C}_3\text{AH}_6$ sequence becomes very blurred; one notes that the effective time-smearing in conventional powder diffraction analysis would effectively extend into hours and therefore it is hardly surprising that there is no real evidence in the conventional cement literature for this important sequence. This example serves as an emphatic reminder of the need for both adequate spatial- and time-resolution when performing *in situ* studies in solid-state chemistry.

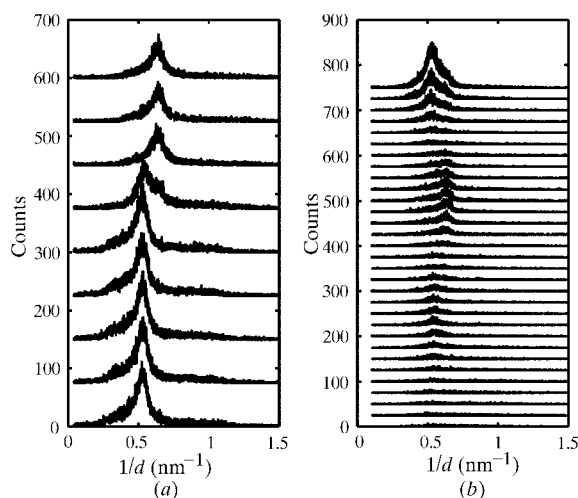


Figure 1

(a) 1 s EDD patterns, spaced 7 s apart in time, showing the rapid change in layer-spacing on addition of KCl to polymer-treated Swy-1 montmorillonite clay suspensions. (b) Variation in layer-spacing in $10\mu\text{m}$ steps down a $\sim 150\mu\text{m}$ -thick montmorillonite film contained within an osmotic cell; the larger $1/d$ between positions 400–600 indicates a decreased basal spacing (equivalent to one water layer) at each side corresponding to the limits of ingress of the KCl during the measurement.

2. The use of penetrating radiation for the *in situ* mode

Traditionally neutron radiation has been the preferred choice of radiation when bulky specimens or complex specimen enclosures are involved. Neutrons retain an

advantage if specimen-bulk averaging is required whereas penetrating X-radiation is preferable when combined time/space-resolution is required. Since the first *in situ* EDD study of autoclave synthesis (Polak *et al.*, 1990; Munn *et al.*, 1992; He *et al.*, 1992), energetic synchrotron radiation has been increasingly used to penetrate specimen cells made of metal (steel, aluminium) or polymer (PEEK) and designed to withstand autoclave conditions, typically 403 to 523 K (more spectacular examples of bulk specimen penetration are presented in §5). Such methodology has now become near-routine and is particularly well subscribed to in the field of synthesis of microporous materials (*e.g.* O'Hare *et al.*, 1998; Clark *et al.*, 1995; Norby *et al.*, 1999; Lewis *et al.*, 1995; Davies *et al.*, 1997; Muncaster *et al.*, 2000) because of the hydrothermal conditions invariably involved and the need for a clear kinetic analysis of the growths of competing products and intermediate phases, with and without template-directing agents. The effective high-energy flux (>100 keV) on third-generation synchrotron sources [*e.g.* at the APS (Shaw *et al.*, 1999) and at the ESRF (Jupe *et al.*, 1996; Hall *et al.*, 1998)] gives further scope for constructing more robust specimen cells. We show here a study example, undertaken at the SRS synchrotron, aimed at understanding cement hydration under conditions typical of oilwell grouting conditions. For this study the oilwell (Portland) cement fills a cylindrical sample cell (8 mm diameter) made of PEEK with a wall thickness of 2 mm. Such studies are of considerable industrial signifi-

cance since the setting behaviour of oilwell cements is crucial to their operation: cements set considerably faster under the high-temperature conditions existing within bore holes yet placement must be completed before setting commences. To achieve this, oilwell cements have a low tricalcium aluminate content and are used with retarding additives. We are now able to compare the hydration behaviour of oilwell cements under ambient and autoclave conditions. Typical data obtained under autoclave conditions are shown in Fig. 3(a) for which the normalized phase-concentration plots are shown in Fig. 3(b); for comparison the phase-concentration plots for ambient hydration are given in Fig. 3(c). Some differences are immediately obvious: the production of calcium hydroxide, often used as an indicator of the progress of setting/hardening in Portland cements, starts much sooner, after 160–170 min compared with 300–400 min under ambient conditions; the brownmillerite phase (calcium aluminoferrite) starts to be consumed within 160–170 min whereas under ambient conditions it remains unaffected; a complex interplay occurs between three calcium aluminosulfate hydrate phases (ettringite $C_3A.3Cs.32H$; 14-water monosulphate $C_3A.Cs.14H$; 12-water monosulphate $C_3A.Cs.12H$; where $s = SO_3$) whereas only one calcium aluminosulfate hydrate, ettringite, occurs under ambient conditions. The effect of the retarders can be easily evinced from hydration experiments under ambient conditions: the calcium hydroxide production is delayed from 300–400 min to

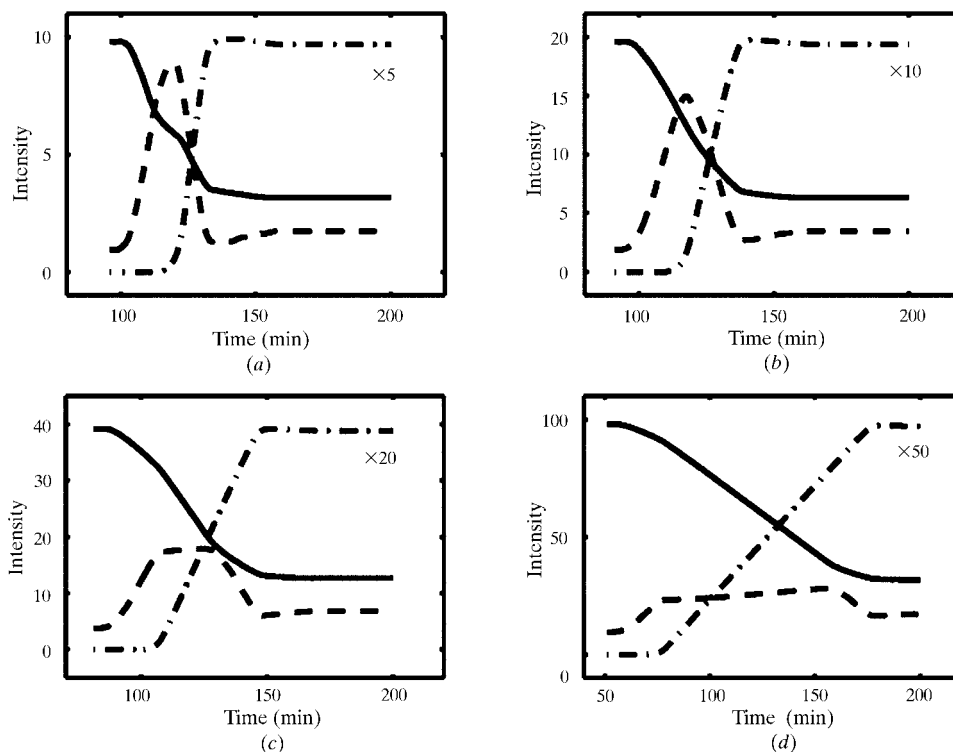


Figure 2

Normalized plots of C_3A hydration (C_3A – continuous; intermediate – dashed; final hydrate – dash/dotted curves) with various degrees of simulated space-time smearing: (a) 5 s, (b) 10 s, (c) 20 s, (d) 50 s. It is clear that once the time-smearing exceeds ~ 50 s, the essential sequence is lost.

beyond the total experimental measurement time (620 min) in the case of two typical retarder types (Fig. 4a), and the consumption profile of ettringite under autoclave conditions is also modified by the same retarders (Fig. 4b). These differences are now being used to test existing ideas regarding the retardation mechanisms involved and to provide a behavioural baseline from which to assess novel retarders. It is difficult to imagine any alternative methodology which could so conveniently and effectively provide *in situ* data on these bulk hydrating systems.

3. Use of complementary and combined *in situ* techniques

The application of several complementary techniques to a single problem is becoming increasingly recognized as an effective means of pooling together different structural views on a chemical/materials event. An excellent review of this approach has been provided by Cheetham & Mellot (1997) where various combinations of diffraction (laboratory, synchrotron X-rays, neutrons), small-angle scattering

(X-rays, neutrons), spectroscopy/resonance methods (X-ray absorption spectroscopy, nuclear magnetic resonance, vibrational spectroscopy) and imaging (optical, electron, atomic force) have been applied to *in situ* studies of sol-gel synthesis processes. A further subset of this approach is to perform two or more complementary techniques simultaneously in time. In the opinion of the authors this further approach is best served by repeating a given experiment in both combined and individual technique mode: the former is necessary to bring the information from each technique into time registration, while the latter ensures that essential information is not marred by the inevitable compromises that have to be made with combined technique stations. A very recent example of the combined technique approach can be seen with the building of the new ten-pole wiggler station on the Daresbury SRS (Cernik *et al.*, 1999–2001) which will combine three techniques, powder X-ray diffraction, small-angle scattering and EXAFS, with multi-wire detector technology capable of capturing data sets within 10 s. In the following we provide three illustrative examples where

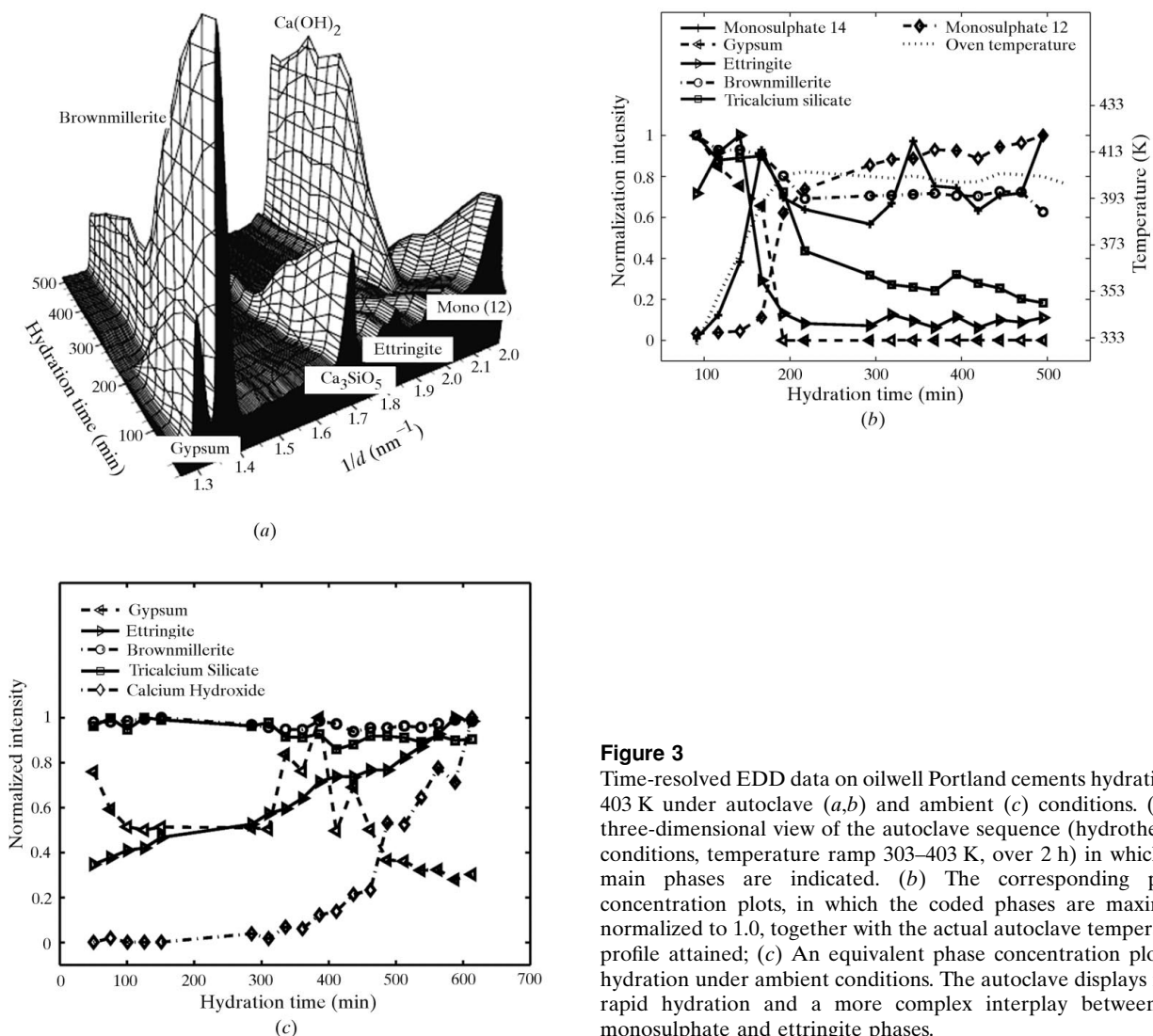


Figure 3

Time-resolved EDD data on oilwell Portland cements hydrating at 403 K under autoclave (a,b) and ambient (c) conditions. (a) A three-dimensional view of the autoclave sequence (hydrothermal conditions, temperature ramp 303–403 K, over 2 h) in which the main phases are indicated. (b) The corresponding phase concentration plots, in which the coded phases are maximally normalized to 1.0, together with the actual autoclave temperature profile attained; (c) An equivalent phase concentration plot for hydration under ambient conditions. The autoclave displays more rapid hydration and a more complex interplay between the monosulphate and ettringite phases.

complementary/combined techniques have provided both challenge and eventual elucidation and in which energy-dispersive diffraction played a central role.

3.1. Calcination of zirconium hydroxide to zirconia

This concerns previously published studies (Turrillas *et al.*, 1995) into the structural and kinetic aspects of this amorphous-to-crystalline reaction-transformation which has now become the subject of visual and computational modelling methods (*Cerius 2 Visualizer*; Molecular Simulations, CA, USA). The raw data obtained from X-ray diffraction, neutron scattering and Zr-EXAFS experiments superficially look very different, with two of these techniques, X-ray diffraction and Zr-EXAFS, having also been performed in combined technique mode on station 9.3 of the SRS. The basic information provided by each technique can be briefly summarized as follows:

(i) X-ray diffraction (both energy- and angle-dispersive modes) gave the least information on the amorphous hydroxide structure, but was the simplest way to gain kinetic data on the amorphous hydroxide to tetragonal oxide and tetragonal to monoclinic oxide transformation as a function of starting material, heating/cooling rate and top temperature.

(ii) Neutron scattering, employed (at ILL and ISIS) with various isotopic/group substitutions (*i.e.* OD⁻/D₂O and CH₃O⁻/CH₃OH for OH⁻/H₂O), was able to provide, from the level of incoherent background scattering, direct information on the combined hydroxide/water content at each stage of the calcination, particularly over the final cooperative oxolation/crystallization stage around 773 K.

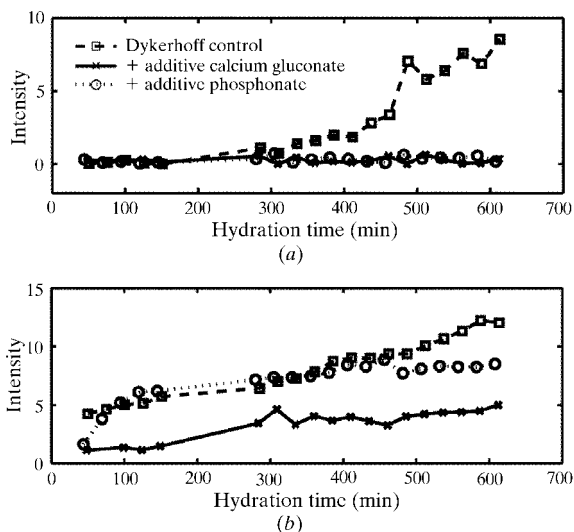


Figure 4

(a) Calcium hydroxide profiles. (b) Ettringite profiles. Data from time-resolved EDD experiments on the hydration of oilwell cement (with and without two typical retarders calcium gluconate; phosphonate) under ambient conditions. The calcium hydroxide production is delayed (a) by the retarders from 300–400 min (without retarder) to beyond the total experimental measurement time (620 min), whereas the change in consumption profile of ettringite is more subtle (b).

(iii) Zr *K*-edge EXAFS, combined with information from the above and the existing literature, was able to interpret the first [Zr–O– at 2.08 Å, Zr–(OH)₂– and Zr–H₂O at 2.16 Å] and second [Zr–O–Zr at 3.27 Å and Zr<(OH)₂>Zr at 3.41 Å] Zr-coordination shells in terms of a generic ‘hydroxide’ two-dimensional nucleating unit.

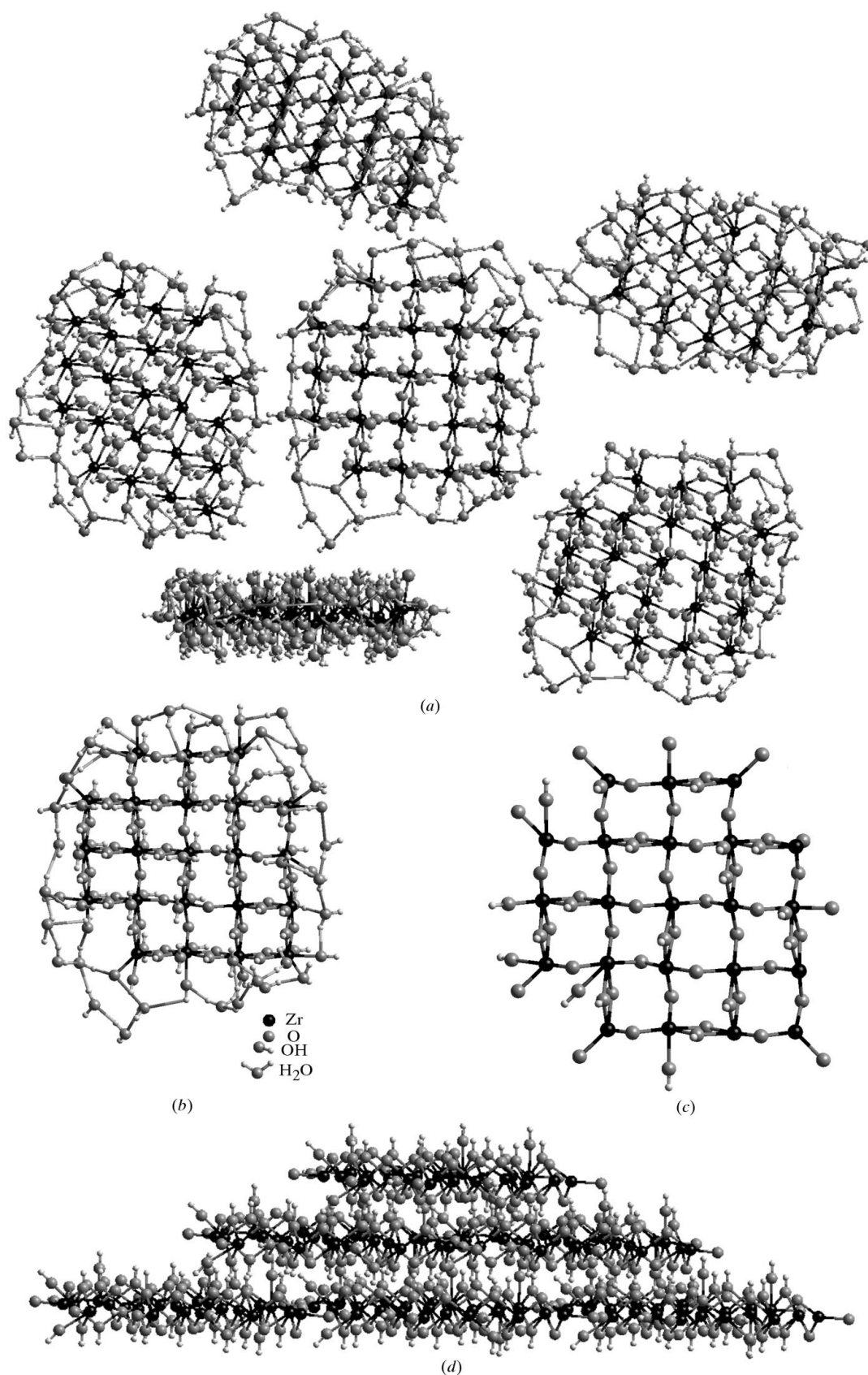
These very different views can be brought together in an illustrative way using the graphic model representations shown in Fig. 5. As such it remains a good example of the elucidating power of multi-techniques.

3.2. The structure and hydration of doped brownmillerites

This case presents a contrasting example to the above in which complementary ‘static’ structural characterization techniques have resulted in partially contradictory views. Brownmillerite is the mineral name given to the calcium aluminoferrite cement phase which has a stoichiometric composition of **C₄AF** (**C** = CaO; **A** = Al₂O₃; **F** = Fe₂O₃) and a perovskite-type structure (Bertaut *et al.*, 1959; Colville & Geller, 1971) in which Al and Fe occupy the tetrahedrally and octahedrally coordinated sites with a statistical preference of 3:1 and 1:3, respectively (Jupe, 1997). However, in real Portland cements (Hall & Scrivener, 1998) the brownmillerite Al:Fe ratio varies and, furthermore, impurities such as Mg and Si substitute for Al and Fe in an, as yet, undetermined way. In an attempt to resolve this latter ambiguity, a combined X-ray/neutron diffraction analysis was performed on a synthetic brownmillerite with composition Ca₄Al_{1.9}Fe_{1.9}Mg_{0.1}Si_{0.1}O₁₀. A combined neutron/X-ray Rietveld refinement procedure has been devised (Jupe *et al.*, 2000) to overcome the under-determinacy resulting from the unknown statistical occupations of Fe, Al and Mg within the structure. This refinement indicates a similar Al,Fe-occupation scheme as that with pure brownmillerite but with the Mg preferring wholly tetrahedral or octahedral, rather than mixed, coordination; the refinement suggests a very slight preference (*i.e.* by tenths of a % in the *R*_{wp}-factor) for the tetrahedral coordination whereas Mg-XANES analysis on station 3.4 of the SRS yields an octahedral XANES signature. That Mg prefers an ordered occupational scheme is interesting given that *in situ* energy-dispersive diffraction shows the Mg-doped brownmillerites to be less reactive than the pure forms (Jupe *et al.*, 2000), suggesting that the Mg adopts a structure-stabilizing role. This example serves as a reminder of the need to confirm ambiguous structural analyses with additional complementary data.

3.3. The high-temperature stability of cation-exchanged clinoptilolite

The behaviour of clinoptilolite, treated with various cation-exchange scenarios, is being studied in order to understand the potential of this naturally abundant zeolite for industrial separation and fixation processes. The treatment stages of interest commence from the as-given clinoptilolite, followed by hydration at ambient conditions, exchange to the cation state of interest, activation by

**Figure 5**

Four computer-graphic illustrations of various stages during the calcination of amorphous zirconium hydroxide to crystalline oxide, as evinced from X-ray/neutron diffraction and Zr-EXAFS data. (a) Initial array of highly hydrated hydroxide units; (b) close up of hydrated hydroxide unit as a defective distorted two-dimensional raft; (c) the same unit after further calcination/dehydration; (d) condensation of rafts at the early stages of three-dimensional crystallization.

calcination (typically to 623 K), and finally thermal destruction (typically 1273 K). The first study was on a mixed Ca,K-cation system and demonstrated the combination of three techniques: high-resolution powder X-ray diffraction, Ca,K-EXAFS and Grand Canonical Monte-Carlo-type computer simulations by which the cation/water content could be varied in order to elucidate likely cation locations as the dehydrated/activated structure was approached; this indicated a valve-type mechanism in which gaseous flow through the zeolite is restricted in either direction by the K cations projecting into the main zeolite channel (O'Connor *et al.*, 1998). The main problem in this study was the poor quality of available clinoptilolite powders: the natural minerals have poor crystallinity whereas the few successfully synthesized versions are multi-phasic, and so the main value of the complementary methods here was rather to compensate for the restricted quality of the experimental data. However, the methodology devised is now being extended to look at other cation combinations, including the Cs form (ideal formula $\text{Si}_{30}\text{Al}_6\text{O}_{22}\text{Cs}_6$) which is implicated in the radioactive ion extraction from contaminated water supplies, and to also examine the intermediate hydration/dehydration stages using rapid combined diffraction/EXAFS facilities (Cernik *et al.*, 1999–2001). An additional interest has now arisen concerning the high-temperature stability of these various systems and a temperature/time-resolved energy-dispersive diffraction protocol is being tested as a rapid comparative method of assessment: the temperature at which crystallinity is destroyed and the detailed diffraction behaviour prior to the structural collapse are found to be quite sensitive to the clinoptilolite type; an example is shown in Fig. 6 for the case of Cs-exchanged clinoptilolite which collapses at 1303 K but with a very distinctive separation of the 130, 400/330 and 240 peaks beforehand. The long-term aims in this kind of study are to be able to model the whole history of these important zeolite systems, during the chemical exchange and hydration/dehydration stages up to eventual collapse and immobilization.

4. Re-analysing previously collected data

Anecdotal evidence suggests that the most rewarding data sets are often those that require many revisits before anomalies are satisfactorily explained. Many examples could be quoted, including the four-year-old study of tricalcium aluminate revisited above. However, we turn to an effect that has defied a satisfactory explanation until recently: this is the anomaly that, with *in situ* time-resolved energy-dispersive diffraction data, the growth/decay curve for a given phase is found to change significantly in shape when recalculated from an alternative h,k,l -peak. Explanations involving crystal size/shape effects are not plausible and, further, the effect persists even when using the same h,k,l -peak at different energies! This latter situation can be conveniently contrived using multi-angle EDD (Barnes *et al.*, 1998) whereby a given h,k,l peak will occur at two

different energies, E_1 and E_2 , according to Bragg's law applied to two different detector angles, $2\theta_1$ and $2\theta_2$,

$$\lambda_1 = hc/E_1 = 2d_{h,k,l} \sin \theta_1,$$

$$\lambda_2 = hc/E_2 = 2d_{h,k,l} \sin \theta_2.$$

If we are examining the same phase, and indeed the same weight fraction $w(t)$ of that phase in the same sample at the same time, t , then the only realistic factors that can alter the growth/decay curves, $I(t)$, with energy are different rates of change in X-ray scattering power or of absorption with density, ρ . This explanation has been stated (Colston *et al.*, 1998) in the following form,

$$I_{E_1}(t) = k_{E_1}w(t)\rho(t) \exp[-a_{E_1}\rho(t)],$$

$$I_{E_2}(t) = k_{E_2}w(t)\rho(t) \exp[-a_{E_2}\rho(t)],$$

where k_{E_i} , a_{E_i} represent unit scattering and absorption at the energy E_i . Taking the logarithm of the ratio of these two equations yields

$$\ln[I_{E_1}(t)/I_{E_2}(t)] = \ln(k) - a\rho(t),$$

where $k = k_{E_1}/k_{E_2}$ and $a = a_{E_1} - a_{E_2}$.

Thus this ratio (or its inverse) reflects the relative change in density with time, $\rho(t)$. Following the initial demonstration of this idea (Colston *et al.*, 1998) the method has been applied to the case of cement hydration with addition of rheology agents to alter the mechanical behaviour (density, viscosity, shear stress) of the hydrating cement. The cement system chosen for study was synthetic (pure) tricalcium silicate (with a water:cement ration of 0.4) with and without four different rheology agents. The various tricalcium silicate decay curves obtained signal anomalous behaviour, in one case even suggesting a growth period during its consumption, which of course is impossible. Such anomalies can only be rationalized in terms of density changes

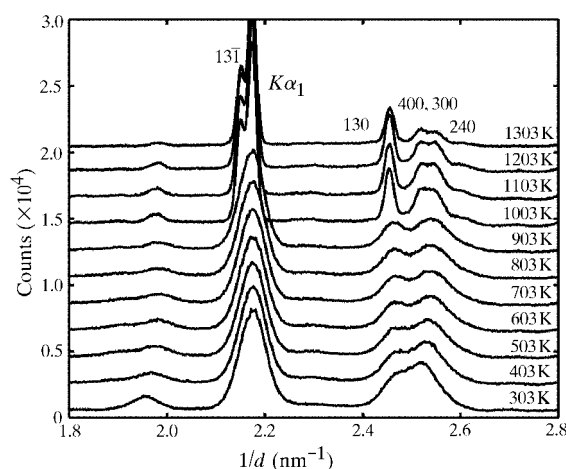


Figure 6

Time/temperature-resolved energy-dispersive diffraction patterns obtained on station 16.4 of the SRS showing the high-temperature behaviour of Cs-clinoptilolite between room temperature and its structural collapse at 1303 K. The distinctive separations of the Cs-fluorescence and 131 diffraction peak and of the 130, 400/330 and 240 peaks are readily apparent.

occurring during hydration. Indeed using the $\ln[I_{E_1}(t)/I_{E_2}(t)]$ method outlined above, for $E_1 = 33.4$ and $E_2 = 51.5$ keV, respectively, for the five cases under study, yields the density curves shown in Fig. 7: all display initial increases in density corresponding to autogeneous shrinkage (which accounts for the false apparent increase in tricalcium silicate content) but thereafter (>4–6 h) show very different behaviour between the control and four additives (see Fig. 7). Density analysis is used in the cement industry, particularly to monitor long-term expansion in concrete which can be deleterious in certain weathering environments (see §5.2 below). However, such tests are performed after at least 24 h and continue over even years of hydration by which time the cement/concrete has acquired sufficient mechanical rigidity and water retention to be compatible with standard hydromechanical methods of measurement. There is no other effective way of extending these density analyses into the first few hours of hydration and therefore the method outlined here is potentially valuable in providing information on the role of different fluidizing systems in relation to hydration kinetics and rheology of silicate cements during the crucial early hydration period.

5. TEDDI: a new kind of (diffraction) tomography

Recently a new kind of tomography, termed TEDDI (tomographic energy-dispersive diffraction imaging) and based on X-ray diffraction, rather than spectroscopic, signals has been realized (Hall *et al.*, 1996, 1998). This has the prospect of yielding, simultaneously, structural information both at the atomic level, *via* the diffraction patterns, and at the macroscopic level *via* the tomographic mode.

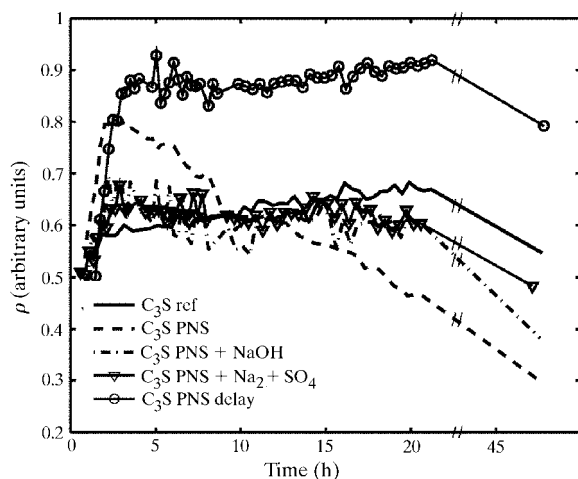


Figure 7

Calculated density–time plots obtained by the method outlined in the text for five cases involving synthetic tricalcium silicate hydration: the pure control system (ref) and four additions of polynaphthalene sulphonate (1% PNS; 1% PNS plus a further 0.64% NaOH; 1% PNS plus a further 1.14% Na_2SO_4 ; 1% PNS plus a deliberately delayed addition of PNS by 45 minutes). After an initial density rise over the first 1–2 h, the density plots show very differing characteristics.

The basic concept is illustrated in Fig. 8 whereby the fixed geometry and tightly collimated incident and diffracted X-ray beams define a small diffraction volume, termed a lozenge. By traversing the sample in one, two or three dimensions the lozenge can be made to visit all required macroscopic regions of the sample and a tomographic map of any diffraction feature (*e.g.* intensity of a given phase h,k,l -peak) can be assembled in the appropriate dimensional space. Also, by using the energetic (20–120 keV) white synchrotron beam, large objects can be penetrated and non-destructively examined; this supplements the point already made in §2 concerning the need for penetrating radiation with *in situ* studies.

TEDDI has some features in common with stress/strain scanning, which has been well practised using both X-ray and neutron sources, where the emphasis is on eliciting unit-cell variations, rather than changes in composition, from the diffraction patterns. The long-standing use of neutron radiation in this context derives from its well known penetrability and atomic/isotopic contrast, and it is only with the more recent wave of second- and third-generation synchrotrons that the alternatives with high-energy X-ray photons are being fully realized (Hall *et al.*, 1998). X-ray scanning devices on third-generation sources are placed to exploit far greater radiation fluxes, but their main advantage lies in the superior X-ray spatial resolution: current neutron scanning devices on spallation and reactor sources (*e.g.* Withers *et al.*, 1995/1996; Webster, 1991) realize spatial resolutions, R , in the millimetre range (or equivalent gauge volumes in the mm^3 range) whereas, for X-rays, R is typically in the tens to hundred micrometre range which is more than sufficient for many practical problems in materials science and engineering, *e.g.* mineralogical cores and geodes ($R = 200 \mu\text{m}$) (Hall *et al.*, 1996); a PEEK phantom defining object (deconvoluted spatial resolution $\sim 1 \mu\text{m}$) (Hall *et al.*, 1998); particulate invasion

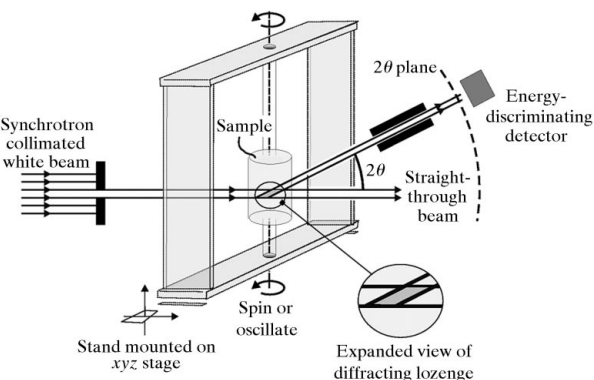


Figure 8

Schematic of the TEDDI principle. The well defined incident and diffracted white X-ray beams define a diffraction lozenge which is also shown in the blow up. By traversing in x -, y - and z -axis directions the diffraction lozenge can be made to visit all required regions of the sample, collecting a stored energy-dispersive diffraction pattern at each region. These patterns are assembled later to form appropriate tomographic images.

through drilling fluids into oil-bearing rocks ($R = 50 \mu\text{m}$) (Bailey *et al.*, 1999); micro-engineering ceramic objects ($R = 25 \mu\text{m}$ over microfeatures) (Colston *et al.*, 2000); archaeological artifacts ($R = 150 \mu\text{m}$) (Barnes *et al.*, 2000).

In this study we report on two new applications, where high resolution is not essential but involve one- and two-dimensional tomographic scanning.

5.1. Super-critical CO_2 attack (one-dimensional TEDDI)

Carbon dioxide at super-critical pressures/temperatures is known to exhibit greatly enhanced activity (diffusion rate; carbonation) and has found many useful applications such as in solvent extraction and cleaning processes. In hydrating cements it is known to have an advantageous effect in which exposed calcium hydroxide in micropores is converted into calcium carbonate thereby reducing the porosity and improving the long-term strength: in fact, the same process, referred to as carbonation, occurs within cements under normal exposure to the environment, but at

much slower rates. In this study, hydrated cement cylindrical rods (typically 8 mm diameter \times 40 mm length) were exposed at each end to supercritical carbon dioxide at $\sim 7 \times 10^6$ Pa and ambient temperature for varied times and subsequently subjected to one-dimensional tomographic examination along the cylindrical axis. The effect becomes pronounced after 60 min as illustrated in Fig. 9. The one-dimensional TEDDI analyses along half the length of the cement cylinder clearly show that the carbonation proceeds as expected from the exposed end [where the $\text{Ca}(\text{OH})_2$ is reduced to the lowest concentration with the CaCO_3 at its highest] to the middle of the cylinder [highest $\text{Ca}(\text{OH})_2$ and lowest CaCO_3]. The reduction in $\text{Ca}(\text{OH})_2$ and increase of CaCO_3 appear to be correlated even to the level of local residual waves (*e.g.* around 1 and 6 mm) on top of the overall CaCO_3 decay. It appears that another crystalline hydrate (ettringite) has also been attacked and the nature of this reaction is currently the subject of further study. This prototype study demonstrates that TEDDI should prove to

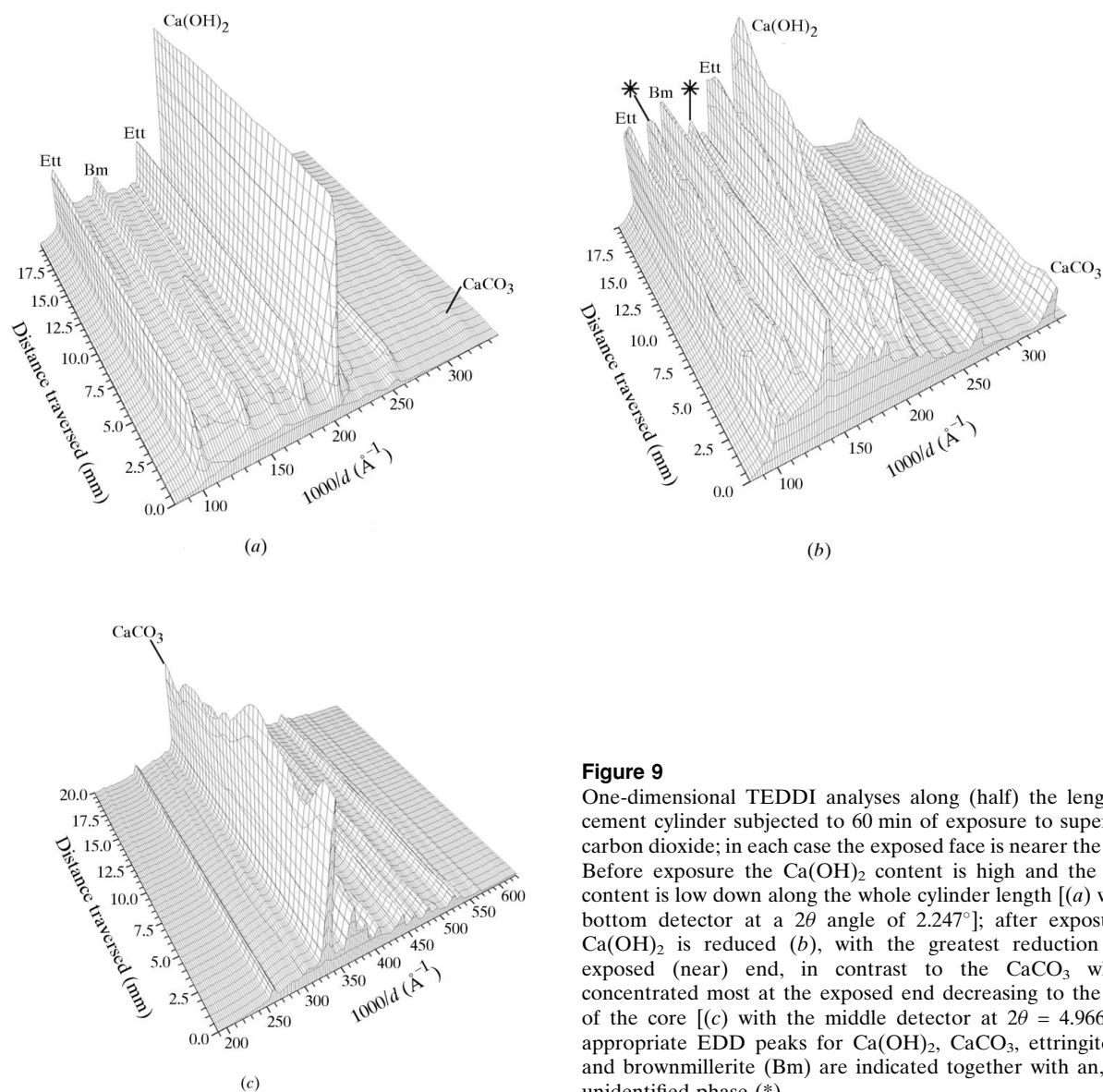


Figure 9

One-dimensional TEDDI analyses along (half) the length of a cement cylinder subjected to 60 min of exposure to supercritical carbon dioxide; in each case the exposed face is nearer the viewer. Before exposure the $\text{Ca}(\text{OH})_2$ content is high and the CaCO_3 content is low down along the whole cylinder length [(a) with the bottom detector at a 2θ angle of 2.247°]; after exposure the $\text{Ca}(\text{OH})_2$ is reduced (b), with the greatest reduction at the exposed (near) end, in contrast to the CaCO_3 which is concentrated most at the exposed end decreasing to the middle of the core [(c) with the middle detector at $2\theta = 4.966^\circ$]. The appropriate EDD peaks for $\text{Ca}(\text{OH})_2$, CaCO_3 , ettringite (Ett), and brownmillerite (Bm) are indicated together with an, as yet, unidentified phase (*).

be a valuable tool in non-destructively charting and assessing the effects of supercritical carbon dioxide in a range of cement types and specimen form.

5.2. Simulated weathering of concrete (two-dimensional TEDDI)

The value of TEDDI for non-destructive applications is apparent in a new study of concrete aging/weathering (Hall *et al.*, 2000). In the example here a large 75×75 mm concrete block has been subjected to simulated weathering by immersion in supersaturated MgCO_3 solution for three months. Particular interest was centred on the presence of ettringite and thaumasite, two related crystalline hydrates which can be the cause for concern if they form/reform in the later stages of concrete life. A two-dimensional TEDDI map was obtained on a selected 8×2.5 mm region just beneath the surface, using the white beam available on station ID30 of the ESRF (the configuration details are given in the caption for Fig. 10). For the purposes of data compression (*i.e.* disk-space limitations *etc.*) only selected windows of the EDD patterns were recorded, around

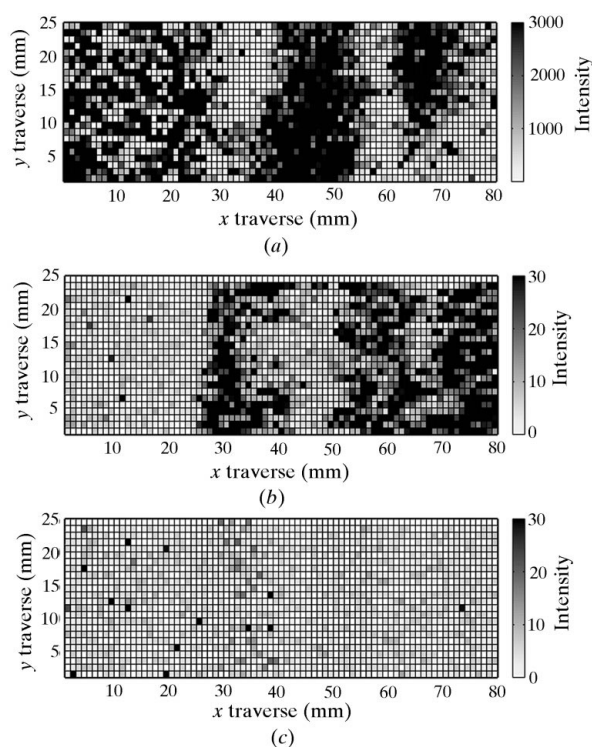


Figure 10

Two-dimensional TEDDI map of a selected $8 \text{ mm} \times 2.5 \text{ mm}$ region just beneath the surface of an artificially weathered concrete block. The incident ($100 \mu\text{m} \times 100 \mu\text{m}$), diffracted ($40 \mu\text{m} \times 100 \mu\text{m}$) beams and detector 2θ angle (3°) result in a diffraction lozenge of area $100 \times 100 \mu\text{m}$ in the plane of the two-dimensional map and length 2.7 mm in the direction perpendicular to the concrete surface. The traverse was performed in steps of $100 \mu\text{m}$ in both directions, thus giving rise to 2000 pixel maps. The three maps given indicate the presence of (a) aggregates (dolomite map), (b) inter-aggregate binding cement hydrate (calcium hydroxide), (c) the ettringite/thaumasite of interest, and how these phases are inter-related.

principal diffraction peaks (two dolomite, one calcium hydroxide and one ettringite and/or thaumasite peak). Owing to the extensive overlap between the ettringite and thaumasite peaks it was not possible to confidently distinguish between these two phases. Fig. 10 shows the occurrence of the aggregate phase (dolomite map), the main hydrate (calcium hydroxide map) and the ettringite/thaumasite phases of interest as a combined map. The location of two fuller and one partial aggregate region is clear from the dolomite map; the calcium hydroxide populates the inter-aggregate regions, which is as might be expected since the cement hydrates that are normally involved in the binding of aggregates within concrete are calcium silicate hydrate (which is mainly amorphous) and calcium hydroxide. The presence of minor hydrates, ettringite/thaumasite, is also indicated. The ability to locate these hydrates, in relation to the aggregate and cement phases, is potentially important since it opens up the possibility of tracking the initiation and progression of these phases over a sustained weathering period in order to increase understanding of their role in environmental weathering. Such information can also be gained by sample sectioning and scanning electron microscopy/X-ray fluorescence analysis, but this would be a destructive one-shot-only approach. With the TEDDI technique there is now the real prospect of revisiting the same interior portions of bulk samples throughout long periods of environmental exposure.

6. Conclusions

This review of current synchrotron studies into the structural and kinetic behaviour of functional ceramic and cementitious materials has highlighted five key points:

(i) Time-resolutions for diffraction, around the 1 s level, appear to be adequate for most solid-state chemical engineering systems of practical interest, provided time-smearing of rate processes within the sample is avoided.

(ii) For energy-dispersive diffraction the penetrating power of an energetic white synchrotron beam (*e.g.* 20–120 keV) is ideal for *in situ* studies: (a) for realizing more advanced specimen environment enclosures, and (b) for non-destructive analysis of the interior of bulk material.

(iii) The use of complementary and simultaneous techniques is encouraged for several reasons: (a) when one technique alone gives a limited view of a process; (b) where a structural solution is under-determined; (c) if the data quality from any one technique is limited on its own.

(iv) The unexpected benefits from re-analysing old data is demonstrated using, as an example, the determination of density *versus* time profiles from multi-angle energy-dispersive data; the method is valid for any evolving system in which the overall chemical composition is homogeneous and conserved.

(v) Well defined penetrating synchrotron white X-ray beams can be exploited to produce a new type of tomographic image based on diffraction rather than spectroscopic signals; the prospect now exists to perform combined

time- and space-resolved diffraction analysis of the interior of bulk solid-state systems during their lifetime and performance.

We wish to thank the sponsoring bodies EPSRC, CLRC (SRS and ISIS), ESRF, ILL, Daresbury Laboratory, The Royal Institution, Schlumberger Cambridge Research (Mr A. Wilson, Professor G. Maitland), Castle Cement Co. (Mr P. Livesey), Fosroc International (Mr J. Dransfield), Italcementi, UMIST (Professor W. Hoff *et al.*), Building Research Establishment (Mr M. Helliwell) and all other associated personnel for their essential and valuable help.

References

- Bailey, L., Boek, E., Jacques, S., Boassen, T., Selle, O., Argillier, J.-F. & Longeron, D. (1999). *Soc. Petrol. Eng.* pp. 471–480.
- Barnes, P., Colston, S. L., Jupe, A. C., Jacques, S. D. M., Cockcroft, J. K. & Hall, C. (2000). *Proc. XVIII Eur. Cryst. Cong.*, Prague, 1998. In the press.
- Barnes, P., Jupe, A. C., Colston, S. L., Jacques, S. D. M., Grant, A., Rathbone, T., Miller, M., Clark, S. M. & Cernik, R. J. (1998). *Nucl. Instrum. Methods Phys. Res. B*, **134**, 310–313.
- Bertaut, E. F., Blum, P. & Sagnières, A. (1959). *Acta Cryst.* **12**, 149–159.
- Boek, E. S., Coveney, P. V., Craster, B. & Reid, P. I. (1998). *Chemistry in the Oil Industry*, Royal Society of Chemistry Special Publication No. 211, edited by L. Cookson, pp. 58–70. London: Royal Society of Chemistry.
- Boek, E. S., Coveney, P. V. & Skipper, N. T. (1995). *J. Am. Chem. Soc.* **117**, 12608–12617.
- Bray, H. J. & Redfern, S. A. T. (1999). *Phys. Chem. Miner.* **26**, 591–600.
- Buttler, F. G., Dent-Glasser, L. S. & Taylor, H. F. W. (1959). *J. Am. Ceram. Soc.* **42**, 121–133.
- Cernik, R. J., Barnes, P., Greaves, G. N., Rayment, T. & Ryan, A. (1999–2001). Unpublished.
- Cheetham, A. K. & Mellot, C. F. (1997). *Chem. Mater.* **9**, 2269–2279.
- Clark, S. M., Nield, A., Rathbone, T., Flaherty, J., Tang, C. C., Evans, J. S. O., Francis, J. & O'Hare, D. (1995). *Nucl. Instrum. Methods Phys. Res. B*, **97**, 98.
- Colston, S. L., Jacques, S. D. M., Barnes, P., Jupe, A. C. & Hall, C. (1998). *J. Synchrotron Rad.* **5**, 112–117.
- Colston, S. L., O'Connor, D., Barnes, P., Mayes, E. L., Mann, S., Freimuth, H. & Ehrfeld, W. (2000). *J. Mater. Sci. Lett.* In the press.
- Colville, A. A. & Geller, S. (1971). *Acta Cryst.* **27**, 2311–2315.
- Craster, B. (1999). PhD thesis, Sheffield Hallam University, UK.
- Davies, A. T., Sankar, G., Catlow, C. R. A. & Clark, S. M. (1997). *J. Phys. Chem.* **B101**, 10115–10120.
- De Siqueira, A. V., Lobban, C., Skipper, N. T., Williams, G. D., Soper, A. K., Performed, R., Dreyer, J. W. & Humphreys, R. J. (1999). *J. Phys. Cond. Matter*, **11**, 9179–9188.
- Fogg, A. M. & O'Hare, D. (1999). *Chem. Mater.* **11**, 1771–1775.
- Glasser, F. & Marinho, M. B. (1985). *Trans. J. Brit. Ceram. Soc.* **35**, 211–236.
- Hall, C., Barnes, P., Cockcroft, J. K., Colston, S. L., Hausermann, D., Jacques, S. D. M., Jupe, A. C. & Kunz, M. (1998). *Nucl. Instrum. Methods Phys. Res. B*, **140**, 253–257.
- Hall, C., Barnes, P., Cockcroft, J. K., Jacques, S. D. M., Jupe, A. C., Turrillas, X., Hanfland, M. & Hausermann, D. (1996). *Analyt. Commun.* **33**, 245–248.
- Hall, C., Colston, S. L., Jupe, A. C., Jacques, S. D. M., Livingston, R., Ramadan, E.-S. & Barnes, P. (2000). *Cem. Concr. Res.* In the press.
- Hall, C. & Scrivener, K. L. (1998). *Adv. Cem.-Based Mater.* **7**, 28–38.
- He, H., Barnes, P., Munn, J., Turrillas, X. & Klinowski, J. (1992). *Chem. Phys. Lett.* **196**, 267–273.
- Jupe, A. C. (1997). PhD thesis, University of London, UK.
- Jupe, A. C., Cockcroft, J. K., Barnes, P., Colston, S. L., Hall, C. & Sankar, G. (2000). In preparation.
- Jupe, A. C., Turrillas, X., Barnes, P., Colston, S. L., Hall, C., Häusermann, D. & Hanfland, M. (1996). *Phys. Rev. B*, **53**, 14697–14700.
- Kolbasov, V. N., Kosyreva, N. A. & Dobronravova, L. A. (1980). *Proc. 7th. Int. Congr. Chem. Cem.* **IV**, 455–459.
- Lewis, D., Sankar, G., Catlow, C. R. A., Carr, S. W. & Thomas, J. M. (1995). *Nucl. Instrum. Methods Phys. Res. B*, **97**, 44.
- Muncaster, G., Davies, A. T., Sankar, G., Catlow, C. R. A., Thomas, J. M., Colston, S. L., Barnes, P., Walton, R. & O'Hare, D. (2000). In preparation.
- Munn, J., Barnes, P., Hausermann, D., Axon, S. A. & Klinowski, J. (1992). *Phase Trans.* **39**, 129–134.
- Norby, P., Christensen, A. N. & Hanson, J. C. (1999). *Inorg. Chem.* **38**, 1216–1221.
- O'Connor, D., Barnes, P., Bates, D. R. & Lander, D. F. (1998). *Chem. Commun.* pp. 2527–2528.
- O'Hare, D., Evans, J. S. O., Francis, R. J., Shiv Halasyamani, P., Norby, P. & Hanson, J. (1998). *Microporous Mesoporous Mater.* **21**, 253–262.
- Polak, E., Munn, J., Barnes, P., Tarling, S. E. & Ritter, C. (1990). *J. Appl. Cryst.* **23**, 258–262.
- Redfern, S. A. T. (1987). *Clay Miner.* **22**, 447–456.
- Roberts, M. H. (1957). *J. Appl. Chem.* **7**, 543–555.
- Ryan, A. (1999). Synchrotron Radiation Satellite Meeting of the XVIII IUCr Congress, 1 August 1999, Daresbury Laboratory, Warrington, Cheshire, UK.
- Shaw, S., Clark, S. M., Wang, T., Henderson, C. M. B. & Shen, G. (1999). *Synchrotron Rad. News*, **12**(3), 21–25.
- Skipper, N. T., Smalley, M. V., Williams, G. D. & Soper, A. K. (1995). *J. Phys. Chem.* **99**, 14201.
- Stein, H. N. (1980). *Proc. 7th. Int. Congr. Chem. Cem.* **IV**, 449–454.
- Svensson, S. O., Birch, J., Müller, H. & Kvick, A. (1997). *J. Synchrotron Rad.* **4**, 83–94.
- Turrillas, X., Barnes, P., Gascoigne, D., Turner, J. Z., Jones, S. L., Norman, C. J., Pygall, C. F. & Dent, A. J. (1995). *Radiat. Phys. Chem.* **45**, 491–508.
- Wark, J. (1999). XVIIIth International Union of Crystallography Congress, 4–13 August 1999, Glasgow, UK. Abstract No. K13.04.007.
- Webster, P. J. (1991). *Neutron News*, **2**(2), 19–22.
- Withers, P. J., Edwards, L. & Johnson, M. W. (1995/1996). *ISIS Annual Report*, Vol. 1, pp. 54–55. ISIS, Central Library of the Research Councils, Rutherford Appleton Laboratories, Chilton, Didcot, Oxfordshire OX11 0QX, UK.